UCTEA Chamber of Geophysical Engineers of TURKEY
Society of Exploration Geophysicists
INTERNATIONAL GEOPHYSICAL CONFERENCE AND OIL & GAS EXHIBITION
ISTANBUL 2012

Uncertainty in microseismic event source locations associated with a fracture stimulation in a tight sand

Sudipta Sarkar, Chevron Energy Technology Company, Andrew Jupe, Altcom Ltd., Julie Shemeta, MEQGeo, Robert Langan, Chevron Energy Technology Company, Anca Rosca, Chevron Energy Technology Company (Now with Magnitude)*

Summary

We present a case study from a microseismic monitoring project during hydraulic fracturing in a tight reservoir in Colorado. Although two monitoring arrays were used to detect the microseismic events during the frac job, the microseismic service provider mostly used one array to locate the events. We performed additional analysis on a selected number of microseismic events to evaluate the potential uplift in location accuracy by using data from both arrays to locate the events. Results from our study show that using two arrays to locate microseismic events for this Colorado stimulation project reduced the major axis of error ellipsoids (uncertainty) by a factor ranging from two to four. We conclude that use of two or more arrays for microseismic monitoring is highly desirable for fracture stimulation monitoring projects.

Introduction

A Chevron business unit collected a microseismic data set in August through October of 2008 in support of a fracture stimulation program for a gas well in a tight sandstone in Colorado, USA. The data were acquired with two, 12-level, 3-C borehole arrays deployed in two other wells in close proximity to the fracture-stimulation well. The geophones were distributed over a 122m interval for one array, and 131m for the other array. The dual-array acquisition design was to ensure that microseismic events would be detected over the full extent of the expected hydraulic fracture geometry for each stage. Using two arrays to image each event location was not part of the original plan.

Thousands of microseismic events were recorded over multiple stages of fracture stimulation, and the moment magnitudes were on the order of -4.0 to -2.5. During the stimulation, the fractures grew vertically and in a nearly East-West azimuth from one stage to another, and were confined to about a 14^{o} azimuthal range. The fracture half-length ranged between 150m and 540m, and their vertical growth was on the order of 165m.

The monitoring arrays during this stimulation job were on the same side of the vertical plane of fracture growth, and the distances from the stimulation well to each array location were considerably different. The distance from the well location of fracture initiation to one array was approximately 160m and the distance to the other array was about 310m.

In order to understand the benefit of using two geophone arrays instead of one array to locate microseismic events, we identified 15 events which were common to both arrays. The events were then located using: 1) the array closest to the stimulation well, and 2) both arrays together.

Method

We used both *P*- and *S*-wave arrivals, combined with *P*- and *S*-velocity models, to determine event locations using (1) the array closest to the stimulation well, and (2) both arrays together. Each location is obtained through forward modeling of traveltimes from an extensive grid of hypothetical locations around the wells. The forward modeling is done with an eikonal traveltime solver. Once a localized region for the location of the event within the grid is determined by how well the modeled times fit the actual time picks throughout the geophone array, an improved location is calculated by interpolating new locations within the grid and forward modeling these trial locations. In the case of single-array locations, the trial grid is confined to a best-fit vertical plane obtained from the hodograms in the array. In the case of the dual-array locations, a 3-D grid is used to fit the traveltime picks in both arrays.

We estimated uncertainties in event locations by using the misfit between modeled traveltimes and actual traveltimes across the array, and assuming that these errors are Gaussian. In the case of the single-array locations, we assumed the differences between the best-fit plane and the azimuth obtained from each hodograms were also normally distributed. We then used the standard deviations of the traveltime misfit and the hodogram misfit as seeds for a Monte Carlo simulation that generated a new set of synthetic traveltime picks and a set of azimuths for the geophone array. Because it is computationally inexpensive to use the same forward modeling approach to determine a hypothetical location for each new simulated data set, we ran the data simulation and forward modeling repeatedly to obtain a distribution of hypothetical locations conditioned by the uncertainties in the traveltimes and hodograms. After calculating a covariance matrix for the spatial locations using this "cloud" of hypothetical locations, we then calculated the 3 eigenvalue/eigenvector pairs from the covariance matrix and used them to define the axes for a best-fit ellipsoid for the cloud. In other words, a form of Principal Component Analysis was used.

In the case of locations obtained using two arrays, we computed a standard deviation for each geophone array to serve as seeds for a similar Monte Carlo simulation and forward modeling exercise. The hodograms play no role in the dual array locations, although they could if one

wanted to determine an appropriate weighting factor for them.

Results

Because the noise floor in the arrays was relatively high, we were able to identify about 50 "pickable" events common to both arrays, of which only 15 events had a high-quality *P*-hodogram on both of the arrays. A hodogram is needed to establish the direction in which the energy is propagating and to uniquely locate an event.

We reprocessed the vendor single-array locations of these 15 events to ensure a consistent processing flow for our single-array and dual-array comparisons. Figure 1 compares in map view the vendor single-array locations to our single-array and dual-array locations. Figure 2 adds the computed uncertainties to Figure 1 and zooms in on the 15 events. Note the very large major axes of the error ellipsoids of the single-array locations in map view. They collapse by about 2/3 when two arrays are used.

Our approach to modeling uncertainties does not capture all the errors associated with locating the events, such as systematic errors in the V_p/V_s ratio. This is evident in our display because even if we were to expand the ellipses to 3 standard deviations, not all the differences between each set of result would be explained by our uncertainties. For example, a slightly different velocity model was used in our processing than what the vendor used.

Figure 3 shows the side view of the event locations, along with the error ellipsoids. The major axes of the error ellipsoids of the two array locations are tilted such that the minor axis is in the direction of Array 1, which is at a different depth from Array 2 and the stimulation zone.

Discussion

The same approach for modeling uncertainties can also be used to help with survey planning, optimizing acquisition strategies, and understanding in advance what the potential limits in location accuracy might be. By defining a preliminary velocity model, making reasonable assumptions about the misfit between picked traveltimes and modeled traveltimes, and estimating the error in the determination of the orientation of a single plane from hodograms (if hodograms are to be used), one can then run a suite of simulations for different acquisition strategies and different candidate event locations at a grid of points in the subsurface. The same procedure as was used in the error analysis can then be applied to obtain error ellipses for synthetic data sets. By plotting the major axes of these error ellipses, one has an effective display of the errors associated with a proposed acquisition geometry in a given project.

Figure 4 is an example of this approach for our Colorado microseismic survey, using the dual array acquisition, the same velocity model, and some assumed traveltime errors. In this example we have plotted the value of the major axis of the ellipse for two standard deviations (95% confidence) on a horizontal slice at the reservoir depth. The most interesting feature is the large uncertainty that exists along a vertical going through the two vertical wells. If we were to expect some microseismic events to occur near this vertical plane, and the expected error in locating them was unacceptable, we would need to add a third monitoring array.

Conclusion

In this study we have shown that using two arrays to locate microseismic events in a fracture stimulation reduces the major axis of the error ellipsoids (for one standard deviation) computed for velocity model and event-picking uncertainties by a factor ranging from two to four. It also eliminates the 180^o uncertainty associated with a single array in determining the side on which the event occurred. This reduction in event uncertainty would also significantly reduce uncertainty in estimates of the stimulated reservoir volume (SRV), a critical measure used to gauge stimulation effectiveness. In addition, by using two arrays we had a more robust processing workflow and it allowed us to perform a limited focal mechanism analysis on some events. Therefore, using two or more arrays to monitor a given fracture stimulation stage is highly desirable and requires some pre-survey planning to determine how best to make use of the wells available for monitoring.

Acknowledgement

We thank Chevron for giving us permission to present the results.

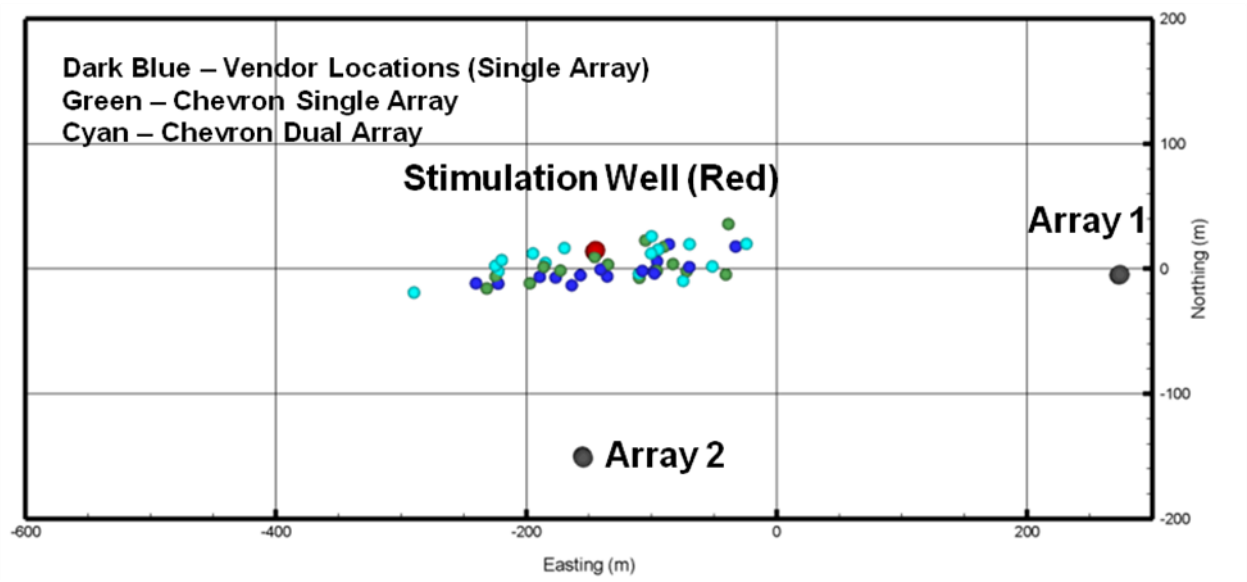

Figure 1: A comparison, in Map View, of vendor-derived single-array microseismic event locations, with our derivation of locations using both the same single array and dual arrays.

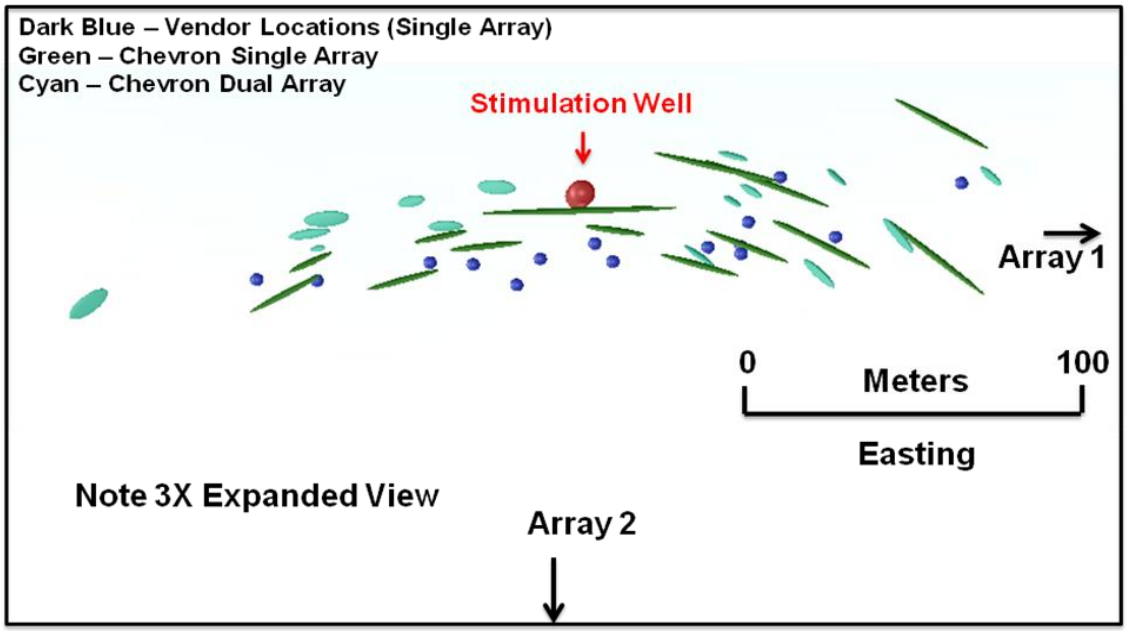

Figure 2: Map View of the same microseismic event locations as shown in Figure 1, with computed uncertainties added. This display in expanded about 3 times over Figure 1.

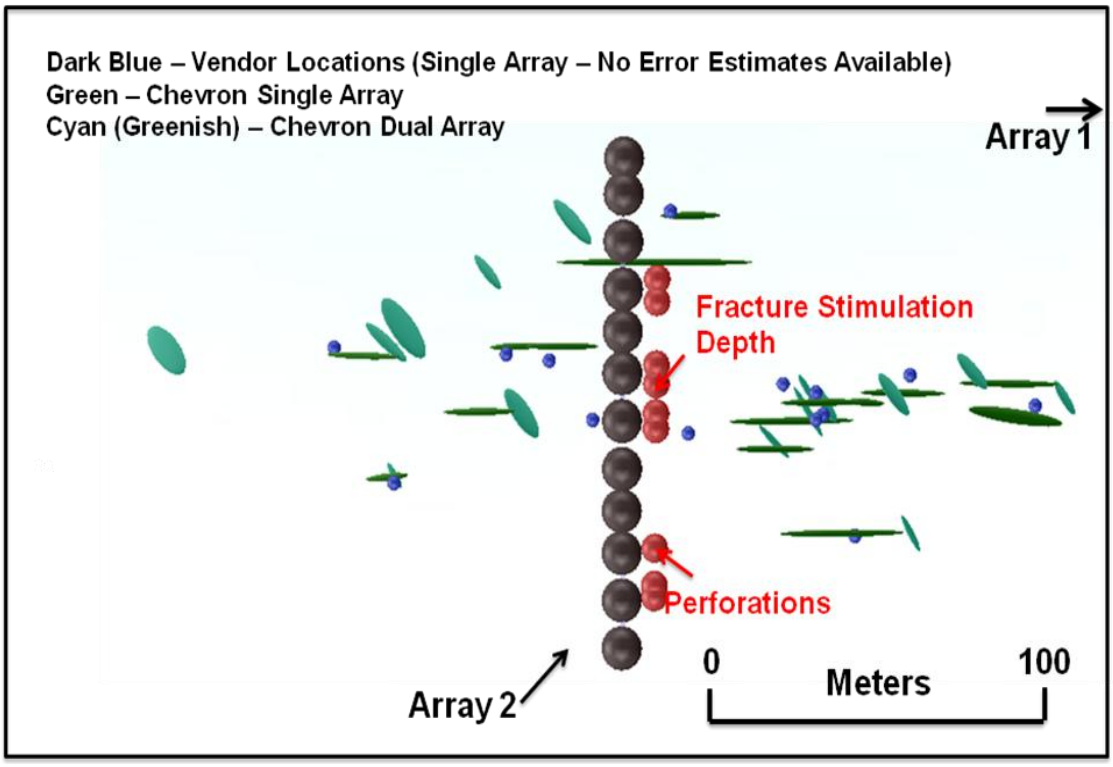

Figure 3: Side view of the same events and uncertainties as in Figure 2. Array 1 is at depth of the arrow, which accounts for the orientation of the major-minor axes in the dual-array locations.

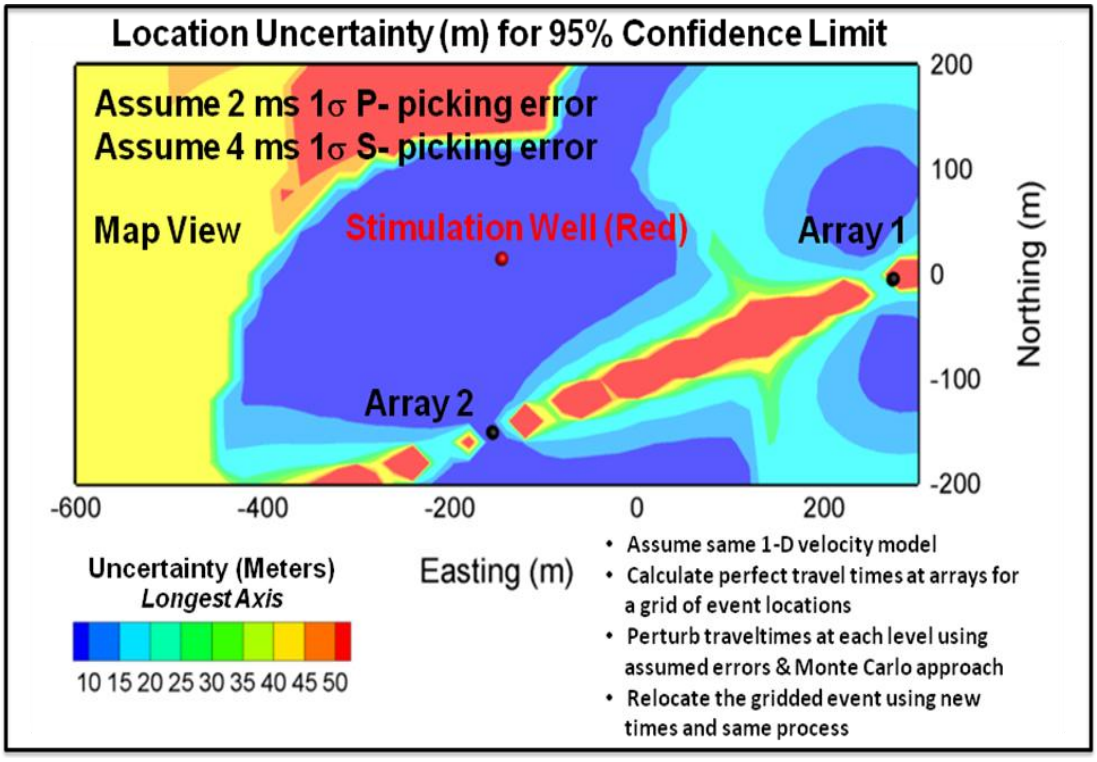

Figure 4: Uncertainties in microseismic event locations on a depth slide at the reservoir level for a "proposed" acquisition geometry. In this case we used the same geophone array locations and velocities as were used in the actual microseismic survey. Note the zone of high uncertainty along a line passing through the two array locations.